Optics and Lasers in Engineering 184 (2025) 108694

Contents lists available at ScienceDirect

Optics and Lasers in Engineering

journal homepage: www.elsevier.com/locate/optlaseng

Double spiral phase filter digital in-line holography for particle field recording and tracking

J. Lobera [a,*], A.M. López Torres [a], N. Andrés [a], F.J. Torcal-Milla [a], E.M. Roche [a], V. Palero [a]

[a] Instituto de Investigación en Ingeniería de Aragón (I3A), Universidad de Zaragoza, Zaragoza, Spain

ARTICLE INFO

Keywords:
Digital holography
Spiral phase filter
Particle imaging
Particle tracking Velocimetry

ABSTRACT

The application of digital in-line holography in fluid velocimetry is mainly limited by the twin image that hinders the particle position and velocity measurements. In this work, we propose the use of two spiral phase filters in a digital in-line holography configuration to discriminate the real and virtual images. The first filter is a physical plate that modifies the object spectrum prior the recording. The second filter is a numerical frequency filter, applied in the reconstruction process, which reshape one of the particle images into a point-like image while blurs its twin image. In this way, particle tracking algorithms, based on the detection of intensity peaks, can easily locate and track particles. The good performance of double spiral phase filter in-line holography for particle field recording and particle tracking has been demonstrated experimentally in the present work.

1. Introduction

Digital holography has been extensively used to characterize fluid flows by determining the movement of tracer particles [1–7]. In particular, digital inline holography (DIH) combined with Particle Tracking Velocimetry (PTV) strategies [3–7] allows the accurate measurement of the particle position and velocity in a volume.

The main advantage of DIH is its set-up simplicity. However, the twin image problem [8] compromises several recording conditions such as focus distance, measurement resolution and, as a consequence, its overall performance for velocimetry applications [6]. Different approaches have been proposed to eliminate the twin image in the analysis after the recording . To improve the reconstructed image of a generic object (extended or punctual object, phase or intensity object), cumbersome iterative methods are usually required [9–11].

Let us remark that for fluid velocimetry the analysis has to be applied to series of holograms, and therefore the analysis should be kept as simple as possible. Also, the recorded object is relatively simple, as it consists in a sparse field of small particles and the meaningful information is just its position, its displacement or its size. The standard and robust location algorithms used for PTV [3–7] consider particles as point scatters whose scattering patterns present a nice local intensity maximum. In order to make an efficient and correct use of the PTV algorithms, the most desirable scenario is to have image particles with sharp intensity peaks.

For those reasons, the noise introduced by the twin image is very often disregarded and DIH-PTV is applied with the only precaution of recording the tracers out of focus to avoid the sign ambiguity. However, recent interest has been focused in removing physically the twin image with a side-band filter [12–13] to improve the SNR of the recording [6]. This technique consists of blocking half of the frequency domain with an intensity filter during the recording. This method removes the twin image without compromising the axial resolution [14], but it affects to one of the components on the transversal plane.

In this paper, we introduce a different approach that, without removing the twin image, contributes to solve the associated problem for particle tracking. It requires the use of two spiral phase filters. One of them is a physical filter that consists in a vortex phase plate that will not limit the system aperture and therefore the spatial resolution either in the axial or the transversal direction. The second one will be used as a digital filter in the image reconstruction.

The spiral phase contrast filters are used in microscopy to improve the visualization of some object features, in the same way as other more popular phase contrast techniques. They consist on a phase or intensity plate placed at the Fourier plane of the imaging system, where they modify the relative phase between the diffracted and non-diffracted light, so the object phase changes turn into intensity changes. In a holographic recording all these enhanced contrast techniques can be considered as 3D filtering operations of the 3D reconstructed object image, which can also be implemented as a digital post-processing [15].

In recent years, there has been an increased use of vortex beams in the recording of digital holograms for different applications: for

* Corresponding author.

https://doi.org/10.1016/j.optlaseng.2024.108694
Received 4 July 2024; Received in revised form 30 September 2024; Accepted 8 November 2024
Available online 16 November 2024

enhanced contrast imaging [16–19], for interferometry [19–21] and for sign disambiguation [22]. In those works, the recorded spatial frequencies are modified by a vortex phase filter, generally implemented into spatial light modulators (SLMs) in a 4f-set-up [19].

We propose to use the spiral phase filter twice: first, as an optical element in the holographic recording to encode the object information; and second, as a digital filter in the image reconstruction of the object to conveniently decode the object information. The important advantage of this method is evident when this second filter is applied, as it allows us to discriminate the real image of a particle form its virtual image. The reconstructed particle images are recovered as nice, narrow peaks, while their twin images have a broad, low-intensity shape, as far from a local maximum as possible. Therefore, only one of the images is accurately identified and tracked as a particle by PTV algorithms thus removing the twin image problem. Furthermore, the higher the topological charge of the vortex filter, the better we expect to be its performance for particle tracking velocimetry.

In this work, we use a modified holographic in-line configuration, that keeps the simplicity of a standard in line holographic set-up. A photographic objective images the particle field near the sensor. Thus, we can access to the spatial frequency spectrum in the back focal plane of the lens, where we can locate a spiral phase plate . This configuration introduces two main advantages: the use of a SLM is not required and it keeps the simplicity of an in-line holographic set-up.

In the following section we will introduce the theoretical bases of this work, by describing the application of any general frequency filter. Then, we will describe the spiral phase filters and the effect of its application both in the holographic recording of the particle image, and on its reconstruction. We will demonstrate that the reconstruction filter allows us to discriminate the real image of a particle form its virtual image. The reconstructed particle images are recovered as nice, narrow peaks, while their twin images have a broad, low-intensity shape. Therefore, only one of the images is identified as particle by PTV algorithms based on the sharpness of the peak intensity, removing the twin image problem. Then, we will present the results on a test object and we will discuss the performance of the proposed technique for particle localization and tracking.

2. Frequency filters used in the holographic recording and reconstruction

The field scattered by an object at a position $\vec{r}$ is a complex function $u(\vec{r})$, which can be decomposed into its spectrum $S\left(\vec{k}\right)$ of wave vectors $\vec{k}$ such as,

$$u(\vec{r}) = \int_{-\infty}^{+\infty} S\left(\vec{k}\right)\exp\left(i\vec{k}\cdot\vec{r}\right)d\vec{k} \tag{1}$$

However as the field propagates, the spectrum is reduced to the wave vectors that comply $|\vec{k}| = k_0 = \frac{2\pi}{\lambda}$ [23–24], were λ is the wavelength of the light source. In addition, the numerical aperture of the system will further limit the spectrum. Thus, for an axial system with finite Numerical Aperture (NA) around the Z-axis, the corresponding transfer function, $H\left(\vec{k}\right)$, can be written [25],

$$H\left(\vec{k}\right) = \frac{1}{k_0^2}\delta\left(\left|\vec{k}\right| - k_0\right) step\left(\vec{k}\cdot\hat{z} - k_0\sqrt{1-NA^2}\right) \tag{2}$$

For any punctual particle, the measured object field will be given by the impulse response or Point Spread Function (PSF) $h(\vec{r})$,

$$h(\vec{r}) = \int_{-\infty}^{+\infty} H\left(\vec{k}\right)\exp\left(i\vec{k}\cdot\vec{r}\right)d\vec{k}. \tag{3}$$

And the measured object field, $o(\vec{r})$, can be expressed as a convolution of the scattered field with the PSF:

$$o(\vec{r}) = u(\vec{r}) \otimes h(\vec{r}), \tag{4}$$

or equivalently in the k-space

$$o(\vec{r}) = \int_{-\infty}^{+\infty} O\left(\vec{k}\right)\exp\left(i\vec{k}\cdot\vec{r}\right)d\vec{k} = \int_{-\infty}^{+\infty} S\left(\vec{k}\right)H\left(\vec{k}\right)\exp\left(i\vec{k}\cdot\vec{r}\right)d\vec{k}. \tag{5}$$

So, the recorded object field in a holographic recording, $o(\vec{r})$, can be considered as the result of a linear filtering operation. If we modify the spectrum of the recorded field, with a certain filter $F\left(\vec{k}\right)$, the resultant field can be expressed as:

$$o_F(\vec{r}) = \int_{-\infty}^{+\infty} O\left(\vec{k}\right)F\left(\vec{k}\right)\exp\left(i\vec{k}\cdot\vec{r}\right)d\vec{k} = u(\vec{r}) \otimes h_F(\vec{r}), \tag{6}$$

where, the modified PSF, $h_F(\vec{r})$, is

$$h_F(\vec{r}) = \int_{-\infty}^{+\infty} F\left(\vec{k}\right)H\left(\vec{k}\right)\exp\left(i\vec{k}\cdot\vec{r}\right)d\vec{k}. \tag{7}$$

In the holographic recording we have the interference between the reference wave $r(x,y)$ and this filtered object beam:

$$I(x,y) = |r(x,y)|^2 + |o_F(x,y)|^2 + o_F{}^*(x,y)r(x,y) + o_F(x,y)r^*(x,y). \tag{8}$$

For in-line holography, these four terms are overlapped in the spatial domain, and we should consider the hologram in the frequency domain, $\Im(I)$. The first term of the equation corresponds to the reference beam, which in DIH is roughly a collimated beam parallel to the optical axis of constant amplitude $|r(x, y)| = r_0$, so its Fourier transform can be approximated by a Dirac delta. The second term uses to have low intensity and can be disregarded. The last terms are the filtered real and virtual images. They are mutually conjugated, and therefore their intensity distribution is symmetrical but otherwise identical:

$$\Im(I) = r_o^2\delta\left(\vec{k} - k_0\hat{z}\right) + \Im\left(|o_F|^2\right)\left(\vec{k}\right) + r_oF^*\left(-\vec{k}\right)O^*\left(-\vec{k}\right) + r_oF\left(\vec{k}\right)O\left(\vec{k}\right). \tag{9}$$

In order to solve the ambiguity problem, we can apply a second filter in the reconstruction procedure. To recover the virtual image of the object, $O\left(\vec{k}\right)$, we have to multiply the Fourier spectrum of the hologram by a frequency filter, $G\left(\vec{k}\right)$, such as $G\left(\vec{k}\right)F\left(\vec{k}\right) = 1$,

$$G\left(\vec{k}\right)\Im(I)\left(\vec{k}\right) = r_o^2G\left(\vec{k}\right)\delta\left(\vec{k} - k_0\hat{z}\right) + G\left(\vec{k}\right)\Im\left(|o_F|^2\right)\left(\vec{k}\right) + r_oG\left(\vec{k}\right)F^*\left(-\vec{k}\right)O^*\left(-\vec{k}\right) + r_oO\left(\vec{k}\right) \tag{10}$$

In the same way, to recover the real image, $O^*\left(\vec{k}\right)$, we should multiply by $G^*\left(-\vec{k}\right)$. Note the similarity between this method and the holographic reconstruction procedure where we use a reconstruction filter and we work in the frequency domain, instead of a reconstruction beam in the spatial domain. The implementation of this procedure is particularly simple and powerful when using a phase filter. In such a case $G\left(\vec{k}\right) = F^*\left(\vec{k}\right)$, and we can solve the twin image problem while keeping the entire frequency spectrum, in comparison with the sideband filter shown in [14].

3. Digital in-line holography with spiral phase filters

3.1. Spiral phase filter

In this paper, we consider spiral phase filters, i.e. $F\left(\vec{k}\right) = V_m\left(\vec{k}\right)$, defined as,

$$V_m\left(\vec{k}\right) = \begin{cases} \exp\left(i\, m\, \varphi\left(k_x, k_y\right)\right) & \sqrt{k_x^2 + k_y^2} > k_0 NA_{DC} \\ a_{DC} & \sqrt{k_x^2 + k_y^2} \le k_0 NA_{DC} \end{cases} \tag{11}$$

where φ can be computed as $\varphi\left(k_x, k_y\right) = \tan^{-1}\left(k_y / k_x\right)$, and m is the so-called topological charge of the spiral filter that determines the number of times its phase acquires the 2π value along a complete circumference. Figs. 1a and 1b show the wrapped phase of spiral filters with $m = 1$ and $m = 2$ respectively with the DC region highlighted in red. An ideal vortex filter has a central region with negligible diameter ($NA_{DC} = 0$) and null transmittance ($a_{DC} = 0$) [20].

3.2. Holographic recording

In a DIH configuration with a lens to image the object near the sensor as shown in Fig. 1c, we can place this physical frequency filter in the back focal plane of the lens. In that case a collimated and aligned illuminating beam would be blocked by the filter central stop at the focal plane, and another beam should be introduced as the reference beam to record a hologram. To avoid this extra complexity in the holographic setup, we could use a custom-made phase plate, with a central region that was not completely opaque and had a finite diameter. Furthermore, a convenient value of a_{DC} would allow us to enhance the higher frequencies associated with the object beam (dashed line in Fig. 1c) with respect to the reference beam intensity (solid area in Fig. 1c). That would improve the recording SNR and represents a clear advantage from the standard in-line recording.

Anyway a more practical solution is to use an off-the-shelf diffractive vortex phase plate. The vortex phase plate that we used has a coating profile similar to a helical staircase that has a very small undefined central region. With this device the blocked area is smaller than the beam waist of the reference beam, and the resultant reference beam has lower mean intensity. The intensity and phase of the reference beam vary slowly over the sensor, but the localization and tracking of the particles is not compromised, as we will demonstrate below.

In any case, the resultant impulse response of our system $h_F(\vec{r})$ of Eq. 7 is determined by the vortex plate:

$$h_{Vm}(\vec{r}) = \int_{-\infty}^{+\infty} V_m\left(\vec{k}\right) H\left(\vec{k}\right) \exp\left(i\vec{k}\cdot\vec{r}\right) d\vec{k} \tag{12}$$

and the measured particle field can be expressed as $o_F(\vec{r}) = u(\vec{r}) \otimes h_{Vm}(\vec{r})$ as in Eq. 6 .

It is worth noting that the holographic recording of out of focus particles has a spiral shape whose direction depends on the sign of z, i.e. the axial position of the particle from the plane on focus [22]. As a consequence, the resultant intensity at the hologram plane should allow us to discriminate the sign of z. Fig. 2 shows a simulation of an in-line holographic recording for a particle slightly defocused. It has been computed with $\lambda = 515\ nm$ and a pixel size of $pix = 3\mu m$ for an opaque particle of diameter $3\mu m$ located at 0.50 mm from the hologram.

When no filter is used, the hologram presents a set of rings whose diameters store the information on the particle size and the distance of the particle image to the hologram plane (Fig. 2a). The interference pattern is identical regardless of the defocusing direction, i.e. whether the particle imaged is in front of or behind the sensor. By introducing the phase filter, the object beam is modified, and each scatter behaves like a vortex. At the hologram, the phase along each of the original rings is modified, and the white fringes become spirals with increasing radius clockwise or counterclockwise depending on the defocusing sign (Fig. 2b and 2c).

3.3. Holographic reconstruction

In general, the pixel size is the parameter that limits the effective aperture of the digital in-line recordings, and therefore their spatial resolution [14]. For our experiment, the expected lateral resolution is $R_x = 3\mu m$ and the longitudinal resolution is estimated as $R_z = \frac{8pix^2}{\lambda} = 0.124mm$. For this reason, a regular particle image is one-pixel size in the XY plane but elongated in the Z-direction.

The hologram of Fig. 2b has information of the distance and the sign of the axial position. However, following the classic reconstruction procedure, we will obtain two similar images for each particle (Fig. 3). Fig. 3a shows the central YZ plane where we can appreciate the presence of both twin images symmetrically distributed from the hologram plane at z=0 mm. Figs. 3b and 3c show a detail of the YX plane where the reconstructed real and virtual particle images are formed. The real image is given by $h_{V1}^*(\vec{r})$, and the virtual image by $h_{V1}(\vec{r})$. They have identical intensity distribution, and they only differ in the phase distribution. At the focus plane they appear small rings that cannot be located properly by algorithms designed to find local maxima.

The use of a second spiral phase filter in the reconstruction procedure solves the ambiguity problem. That is, if we consider $G\left(\vec{k}\right) = V_{-m}\left(\vec{k}\right)$ in Eq. 10, the twin images are altered differently. First, for low frequencies, the filter behavior depends on the value of a_{DC}. If $a_{DC} = 0$, $V_m\left(\vec{k}\right)$ blocks low frequencies and removes most of the first two terms of Eq. 10. Furthermore, from the vortex filter definition, one can infer that $V_{-m}\left(\vec{k}\right) = V_m\left(\vec{k}\right)^*$, and $V_m^2\left(\vec{k}\right) = V_{2m}\left(\vec{k}\right)$. Also, for high frequencies $V_{-m}\left(\vec{k}\right)V_m\left(\vec{k}\right) = V_{m=0}\left(\vec{k}\right) = 1$, so $V_0\left(\vec{k}\right)$ behaves as a Dark Field filter. As a result, the hologram spectrum modified by $V_{-m}\left(\vec{k}\right)$ can be expressed as:

$$V_{-m}\left(\vec{k}\right)\Im(I)\left(\vec{k}\right) \approx V_{-2m}\left(\vec{k}\right)O^*\left(\vec{k}\right) + V_0\left(\vec{k}\right)O\left(\vec{k}\right) \tag{13}$$

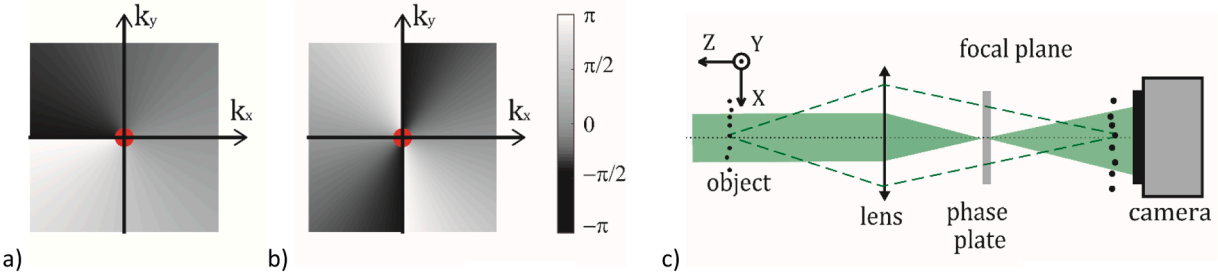

Fig. 1. Phase distribution of a spiral phase plate with topological charge of a) m=1 and b) m=2; c) Schematic drawing of the experimental recording set-up.

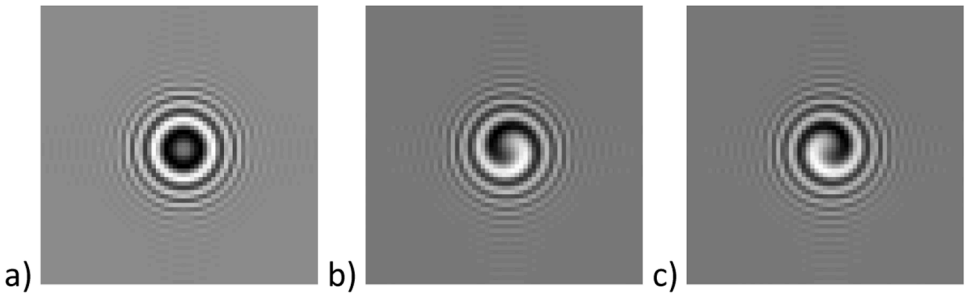

Fig. 2. Numerical hologram of an opaque particle computed: a) without spiral phase filter when the particle is located at z = -0.5 mm; with a m=1 spiral phase filter when the particle is located (b) at z = - 0.5 mm and (c) at z = + 0.5 mm.

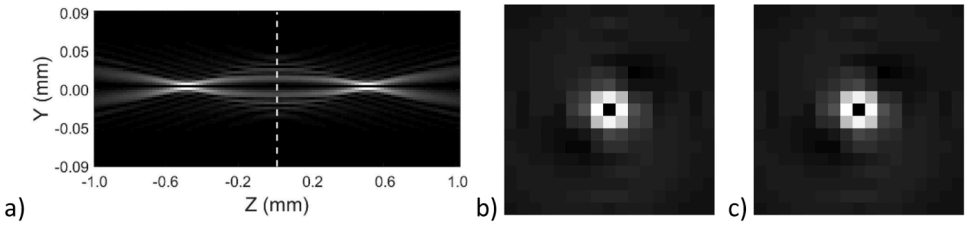

Fig. 3. Reconstructed intensity from a hologram of a particle at $z = -0.5\ mm$ from the hologram, recorded with a m=1 vortex filter and reconstructed without filter: a) central plane YZ; b) YX plane at $z = -0.5\ mm$ and c) YX plane at $z = +0.5mm$.

The PSF of the virtual image, $h_{V0}(\vec{r})$, which is the original PSF minus the low frequency PSF [15]. The smaller NA_{DC} is, the closer $h_{V0}(\vec{r})$ and $h(\vec{r})$ are. For convenience, we choose the DC stop as small as possible but still large enough to remove completely the background illumination. Note that to locate particles from an in-line hologram without filters, the reference beam must also be removed, and this is usually done with a high-frequency filter. For all those reasons, the virtual image of a punctual particle is very similar to those obtained with standard DIH, and it is therefore appropriate for any location algorithm designed for such particle images. Meanwhile the unwanted real image will appear distorted by a spiral phase filter with a topological charge of *-2m*. Thus, the energy of the twin image is diluted into a donut-shaped structure according to $h_{V-2m}(\vec{r})$, which will be much easier to discard by particle location algorithms.

Fig. 4 shows the resultant reconstructed intensity obtained with this procedure from the hologram recorded with the m=1 spiral phase filter (Fig. 2b). The virtual image is focused at z<0 and its shape is given by $h_{V0}(\vec{r})$, which is very similar to the particle image expected in absence of filter. Meanwhile the real image, which can be found at z>0, appears as a ring with much lower intensity. Its actual shape corresponds to $h_{V-2}(\vec{r})$ (Fig. 4c).

In the same way, to turn the real image into a nice peak, the original spiral phase filter, $V_m\left(\vec{k}\right)$, should be used to modify the spectrum of the hologram before numerical propagation.

3.4. Vortex topological charge effect

The same principle could have been applied with other phase filters with different design, and the virtual image would still be nicely recovered with this procedure. Our particular interest on the vortex filter is due to what happens with the twin image. Let us note that, most standard and robust PTV algorithms are mainly based on the sharpness of the intensity peaks to locate particles. Thus, for particle tracking, it is desirable a filter that could also shatter the twin image, i.e. a filter that produces an image as far from a local maximum as possible when applied twice. For that purpose, the spiral phase filters seem particularly suitable. Furthermore, the higher the topological charge of the vortex filter, the better we expect to be its performance for particle tracking velocimetry.

We have simulated the behavior of spiral phase filters with m=2. The resultant hologram presents as many arms or white spiral stripes as the topological charge (Fig. 5a). After applying a m=-2 vortex filter in the reconstruction, the intensity distribution at the central YZ plane (Fig. 5b) shows just one local peak. Fig. 5c and Fig. 5d show the YX planes, where the real and virtual images are located. The reconstruction of the virtual image is identical as in Fig. 4, but the twin image has decreased notably its maximum intensity as it is distributed in a wider region. In particular, the relative intensity of the twin image is around 35% using a m=1 filter, and decrease to a 25% with m=2.

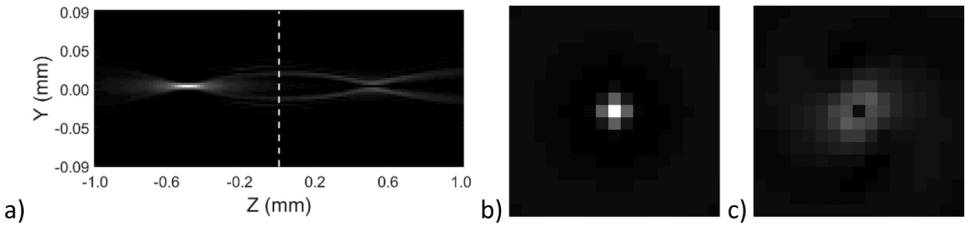

Fig. 4. Reconstructed intensity from a hologram of a particle at $z = -0.5\ mm$ from the hologram, recorded with a m=1 vortex filter and reconstructed with a m=-1 vortex filter: a) central plane YZ; b) YX plane at $z = -0.5\ mm$ and c) YX plane at $z = +0.5mm$.

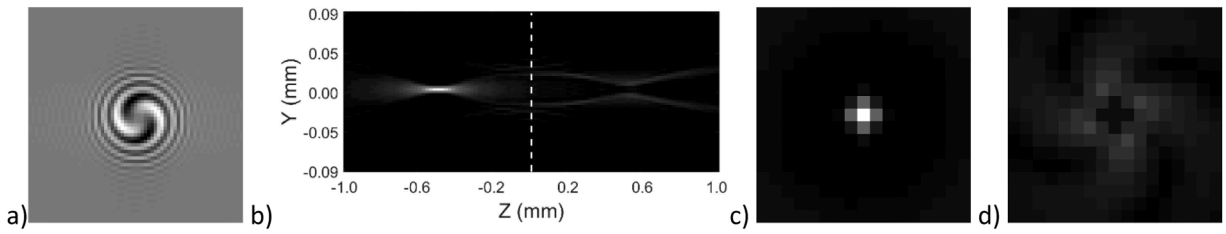

Fig. 5. a) Hologram with a m=2 spiral phase filter of a 3μm particle at z=-0.5 mm from the hologram, and reconstructed intensity with a m=-2 filter; b) central plane YZ; c) YX plane at z=-0.5 mm and d) YX plane at z=+0.5mm.

4. Experimental validation

The capabilities of the spiral phase filter to encode and decode particle field information were evaluated using a test object made with a standard microscope slide and 3μm particles sprinkled on its surface. The object is illuminated by a collimated laser beam ($\lambda = 515\ nm$) and imaged near or on the sensor with a photographic objective (Fig. 1c). A region of $6.1\ mm \times 7.2\ mm$ is recorded in a 2160 × 2560 CMOS sensor with 6.50 μm square pixels. Thus, the pixel size in the object space is $pix = 2.83\ \mu m$. Particles occupy one pixel when on focus and they can be considered as point particles. The photographic objective has a focal length of f`=105 mm and, for our magnification factor, M=2.30, the area in its focal plane, i.e. the frequency plane, that can be effectively recorded is 19 × 19 mm^2. Two 20 mm squared vortex plates with a transmittance efficiency of 93% and topological charge of m=1 and m=2 have been evaluated.

The non-scattered illuminating beam, i.e. the reference beam of the hologram, is focused on the center of the focal plane, where the spiral phase plate has not a defined phase shift due to the fabrication process limitations. The beam waist is larger than the undefined central area and the reference beam passes through the plate with a lower mean intensity. The resultant reference beam has a slowly variable intensity, but it is smooth enough to allow the recording of the particle information in the holograms.

Several holograms were recorded without and with each of the spiral phase plates. Fig. 6 shows an amplified area of those recordings with around twenty particles. These particles are roughly at z = 1.7 mm from the hologram plane and its diffraction pattern occupies a circle with a diameter of around 50 pixels. Thus, in spite of the electronic spurious noise and the overlapping of some diffraction patterns, they can be identified easily.

For each individual particle, we can appreciate the expected ring when no filter is used (Fig. 6a), the spirals when a m=1 vortex plate is used (Fig. 6b) or the double spiral fringes when a m=2 vortex plate is used instead (Fig. 6c).

To control the particle position, the glass slide was rotated around the vertical axis (Y), so that its normal direction makes different angles with the optical axis (Z). To recover the particle information from the holograms we follow the procedure explained in section 3. We applied the corresponding reconstruction filter in the Fourier domain and recover the complex amplitude at the hologram plane. Then, we can compute the image of the particle field at any plane of the studied volume with the Angular Spectrum method [23].

The particles are located by the algorithm described in Lopez *et al.* 2024, which is outlined in the following. In order to avoid an unnecessary increase on the computation time and memory requirements, the particle images are located in two steps: first the complex object field is reconstructed along 7.00 mm in the axial direction. We used a sampling between consecutive planes of 60 μm. Then, we divide the volume in several interrogation windows with 26 × 26 pix^2 section and 7.00 mm depth, and we search for the absolute intensity maximum in each of them. In a second step, the reconstructed image is computed around these initial location estimations. The final position is obtained by fitting the intensity data to a quadratic function of the coordinates. If this position is far from its initial estimation, the peak is removed from the set. This last step allows discarding all the peaks that do not behave as a nice local maximum, usually spurious peaks. In our case, it will also discard the particle twin images, since they will have a donut-shape.

Figs. 7a-c show the ZX particle position obtained this way from one hologram, recorded with a m=1 spiral phase filter and reconstructed with different filters. The microscope slide is placed so its normal direction makes an angle of $\theta = 20^{\circ}$ with the optical axis. There are around 1700 particles between z=-2.5mm and 2.5mm and within the field of view.

If no phase filter is used in the reconstruction, we still need to remove the background intensity which can be achieved using a high-pass intensity filter. In this case, both twin images have the same chances of being found by the location algorithm (Fig. 7a). This result is similar to the expected outcome when no phase filter is used during the recording either, as there is still ambiguity in the sign of z.

However, if a m=-1 spiral phase filter is used in the reconstruction procedure, only the particle virtual images are located (Fig. 7b). In the same way, when a m=1 reconstruction filter is used instead, the position obtained corresponds to the particle real images (Fig. 7c). The resultant

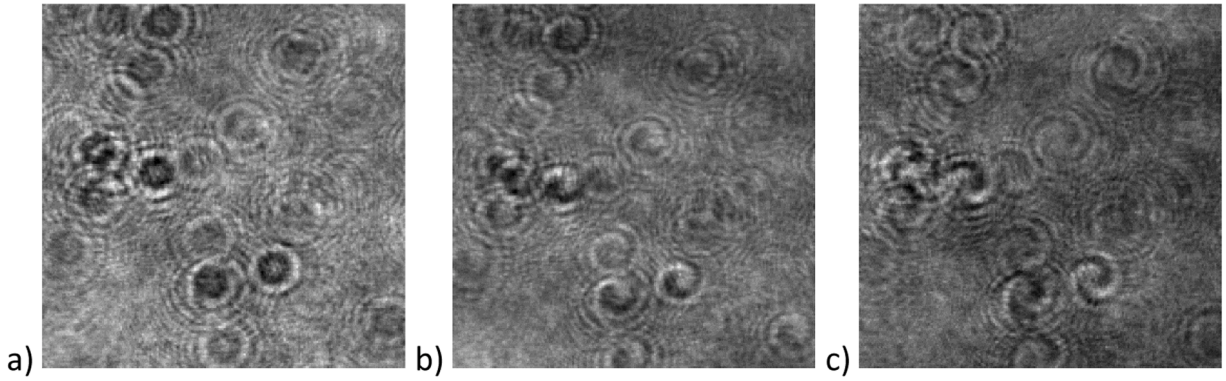

Fig. 6. Amplified area of 200 × 200 pix^2 of holograms recorded a) without filter and with spiral phase filter with b) m=1 and c) m=2.

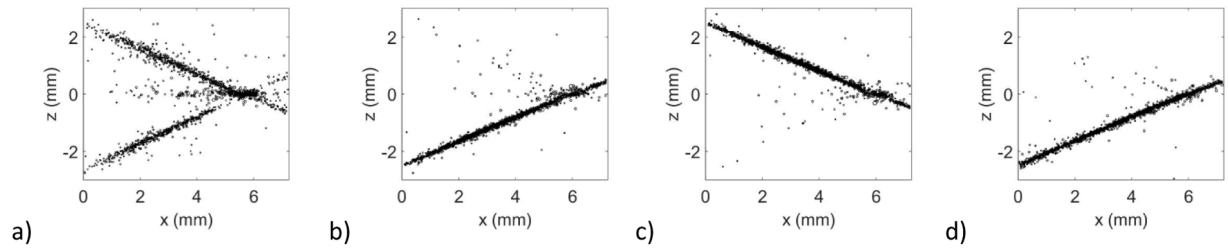

Fig. 7. ZX particle position obtained from a hologram with a recording m=1 spiral phase filter, and a reconstruction with: a) a high pass intensity filter; b) a m=-1 spiral phase filter and c) a m=+1 spiral phase filter; d) ZX particle position obtained from a hologram with a m=2 recording filter and a m=-2 reconstruction filter.

graph is a specular reflection of Fig. 7b as they are the same particles located at the opposite side of the hologram.

In Fig. 7b (and 7c), located particles are found on the plate plane, though some spurious peaks appear at the position expected for the virtual images. Most of these ghost particles are around x=6mm, where particles images are closer to the sensor. When particles are imaged very close to the sensor, the size of those patterns in the hologram are compressed to very few pixels, downsampling its recording. We have chosen to test the technique in those challenging circumstances, when the recorded information of the particle is compromised by the digital nature of the sensor. In this region, particle information is restricted to a few pixels and the electronic noise is more relevant. More importantly, both twin images are overlapped for defocusing distances below the particle axial size. This problem can be reduced with higher order spiral filters. Fig. 7d shows the particle location when using a m=2 spiral phase filter during the recording and a m=-2 filter during the reconstruction.

Continuing with the PTV analysis, once the particles are located, their displacement between two holograms can be obtained with an algorithm based on cross-correlation [5]. For each particle, we reconstruct the complex object field in two small interrogation windows centered at the initial particle location on the first and the second consecutive exposures. Then, if we compute a 3D cross correlation between them, the 3D location of the resultant peaks can be related with the 3D particle displacement. Once we have an estimation of the particle displacement from this initial cross-correlation, we can reduce the interrogation window and compute another 3D cross-correlation to improve the displacement measurement. In particular, we do perform an initial intensity cross correlation with interrogation windows of $60 \times 60 \times 20$ voxels of $3 \times 3 \times 40\ \mu m^3$ along the X, Y and Z direction respectively; a second intensity cross correlation with an interrogation window of $10 \times 10 \times 16$ voxels of $3 \times 3 \times 20\ \mu m^3$ and a third complex amplitude cross-correlation of $8 \times 8 \times 6$ voxels of the same size.

To test the performance of the technique, we introduced a controlled displacement by rotating the plate 4° around the Y-axis. The rotation axis is also within the field of view, so we can study the performance of the technique with very small displacements in the axial direction, Δz. The results obtained with m=1 and m=2 spiral phase filters are presented in Fig. 8a and 8b respectively. As expected, the measured displacement is proportional to the position x with respect to the axis of rotation.

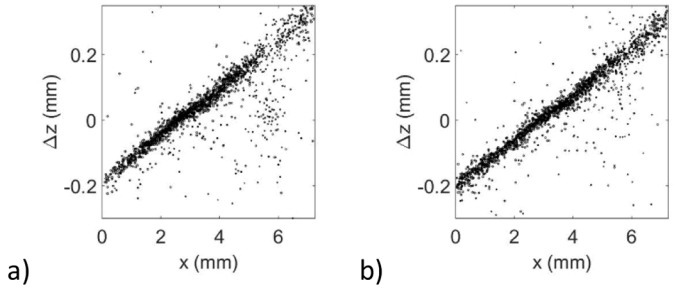

Fig. 8. Axial particle displacement obtained from a hologram recorded and reconstructed two spiral phase filters: a) m=1; b) m=2.

We can appreciate the good performance of the technique for nearly zero displacements at x=3 mm. Meanwhile, where the particles are in focus, there is a significant number of outsiders. In the case of m=1, around x=6mm, the small displacement and small defocus distance make the contribution of the twin image non-negligible within interrogation windows used during cross-correlation. Once again, this problem is reduced with a m=2 spiral filter (Fig. 8b).

Finally, to quantitatively compare the performance of DIH with and without the spiral filter, another set of experiments was performed. Similar holograms were recorded after shifting the microscope slide about 1.5 mm to ensure that all particles were out of focus. In this way, twin images can be discriminated restricting the particle location to negative z values even when no filter is used during the recording.

To calculate the error in the axial position (Z-coordinate), we fit the 3D particle positions to a planar distribution. For each lateral position (XY-coordinates), the nominal axial position must lie in this plane. In this way, the difference between the measured and nominal axial position, z_{error}, can be estimated. The histograms of z_{error} and its standard deviation (STD) are presented in Fig. 9 (top).

Since the displacement is a small rotation, the measured displacement can be also fitted to a linear dependence with XY coordinates. Thus, nominal Δz can be computed from particle lateral positions. Histograms of the difference between the measured and nominal axial displacement, Δz_{error}, and its STD are shown in Fig. 9 (bottom).

The comparison between the STD values shows that the use of spiral filters reduces the measurement error by 37% in axial position and by 56% in axial displacement. Background noise, coming from the out-of-focus twin particle images, makes it difficult to localize and track particles when no filter is used, even if we introduce a defocus distance to discriminate between twin images. We have obtained similar error estimation for both spiral filters, with a slightly better performance of the m=2 spiral phase filter, as also occurred in the experiments of Figs. 7 and 8.

Conclusions

The advantages of using two spiral phase filters to eliminate the twin image problem in digital in-line holography for velocimetry applications has been demonstrated. The first filter is an optical element introduced in the recording. It encodes the object information and breaks the similarity between the twin images. In the reconstruction, a second digital filter is applied to decode the information stored in the hologram spectrum. The proposed strategy reminds how a reconstruction beam decodes the information stored at the hologram intensity distribution, but working in the frequency domain.

The double use of spiral phase filters allows us to recover nice intensity peaks that are required for most standard and robust PTV algorithms. It also transforms their twin images without actually removing them. Spiral phase filters are especially suitable for this procedure for two main reasons. They are phase filters, so the entire spectrum is kept and, in addition, they modify the unwanted twin images into large, low intensity distributions, which can be easily discarded. Besides, our

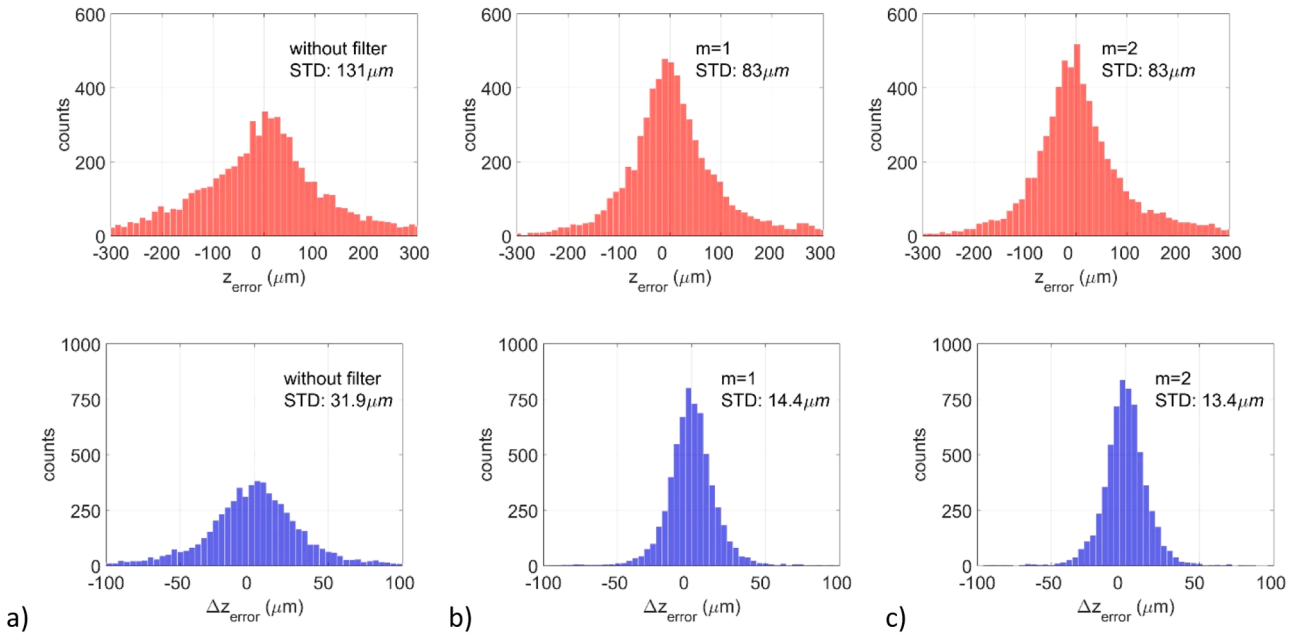

Fig. 9. Histograms of errors in axial positions (z_{error}) and displacements (Δz_{error}) for the cases: a) without filter, b) with m=1 spiral phase filters and c) with m=2 spiral phase filters.

method does not require cumbersome iterative algorithms, as it is just a frequency filter, that can be even incorporated in the propagation algorithm.

The feasibility of the technique to provide accurate particle position and displacement has been proved. It has been particularly discussed the axial coordinate and displacement measurements when particle images are close to the hologram plane and they have small displacements. Experiments have been carried out with two types of vortex of topological charges m=1 and m=2. We have obtained very promising results for both filters although, when the particles are imaged very close to the sensor, the use of m=2 spiral phase filters outperform those of m=1. The experimental error measurement shows an improvement of 37% in axial position and 56% in axial displacement from the DIH without filters.

CRediT authorship contribution statement

J. Lobera: Writing – review & editing, Writing – original draft, Software, Formal analysis, Conceptualization. **A.M. López Torres:** Writing – review & editing, Validation, Investigation. **N. Andrés:** Writing – review & editing, Resources, Funding acquisition. **F.J. Torcal-Milla:** Writing – review & editing, Validation. **E.M. Roche:** Investigation, Data curation. **V. Palero:** Writing – review & editing, Visualization, Resources, Methodology, Funding acquisition.

Declaration of competing interest

The authors declare that they have no known competing financial interests or personal relationships that could have appeared to influence the work reported in this paper.

Acknowledgments

This study was funded by MCIN/AEI/10.13039/501100011033 and FEDER program through the grants PID2020-113303GB-C22 and PID2023-146648NB-C22, and by Gobierno de Aragón-FEDER through Grupo de Tecnologías Ópticas Láser - E44_23R.

Data availability

Data will be made available on request.

References

[1] Arroyo MP, Hinsch KD, Recent Developments of PIV towards 3D Measurements. Ed. A. Schroder, C.E. Willert, Springer, New York, 2008, p. 127.
[2] Katz J, Sheng J. Applications of holography in fluid mechanics and particle dynamics. Annu Rev Fluid Mech 2010;42:531.
[3] Pu SL, Allano D, Patte-Rouland B, Malek M, Lebrun D, Cen KF. Particle field characterization by digital in-line holography: 3D location and sizing. Exp Fluids 2005;39:1–9.
[4] Memmolo P, Miccio L, Paturzo M, Di Caprio G, Coppola G, Netti PA, Ferraro P. Recent advances in holographic 3D particle tracking. Adv Opt Photon 2015;7:713.
[5] López AM, Lobera J, Andrés N, Arroyo MP, Palero V, Sancho I, Vernet A, Pallarés J. Advances in interferometric techniques for the analysis of the three-dimensional flow in a lid-driven cylindrical cavity. Exp Fluids 2020;61:10.
[6] López AM, Lobera J, Andrés N, Subías A, Roche EM, Torcal-Milla FJ, Arroyo P, Pallarés J, Palero V. Double field of view digital sideband holography as an optimized method to measure velocity fields in a large fluid volume. Opt Lasers Eng 2024;175:107993. https://doi.org/10.1016/j.optlaseng.2023.107993.
[7] Toloui M, Mallery K, Hong J. Improvements on digital in-line holographic PTV for 3D wall-bounded turbulent flow measurements. Measurem Sci Technol; 2017;28: 044009. https://doi.org/10.1088/1361-6501/aa5c4d.
[8] Guizar-Sicairos M, Fienup J. Understanding the twin-image problem in phase retrieval. J Opt Soc Am A 2012;29:2367–75.
[9] Denis L, Fournier C, Fournel T, Ducottet C. Numerical suppression of the twin image in in-line holography of a volume of micro-objects. Meas Sci Technol 2008; 19:074004.
[10] Zhang W, Cao L, Brady DJ, Zhang H, Cang J, Zhang H, Jin G. Twin-image-free holography: a compressive sensing approach. Phy Rev Lett 2018;121(9):093902.
[11] Latychevskaia T. Iterative phase retrieval for digital holography: tutorial. J Opt Soc Am A 2019;36:D31–40.
[12] Palero V, Lobera J, Andrés N, Arroyo MP. Shifted knife-edge aperture digital in-line holography for fluid velocimetry. Opt Lett 2014;39:3356–9.
[13] Ramírez C, Lizana A, Iemmi C, Campos J. Inline digital holographic movie based on a double-sideband filter. Opt Lett 2015;40:4142–5.
[14] Lobera J, Palero V, Roche EM, Gómez-Climente M, López-Torres AM, Andrés N, Arroyo MP. Tilted illumination in-line holographic velocimetry: improvements in the axial spatial resolution. Opt Lasers Eng 2020;134:106280.
[15] Lobera J, Coupland J M. Contrast-enhancing techniques in digital holographic microscopy. Meas Sci Technol. 2008;19:025501. https://doi.org/10.1088/0957-0233/19/2/025501.
[16] Fürhapter S, Jesacher A, Bernet S, Ritsch-Marte M. Spiral phase contrast imaging in microscopy. Opt Expr 2005;13:689–94.
[17] Zhou Y, Feng S, Nie S, Ma J, Yuan C. Image edge enhancement using Airy spiral phase filter. Optics Expr 2016;24(22):25258.
[18] Ritsch-Marte M. Orbital angular momentum light in microscopy. Phil Trans R Soc A 2017;375:20150437.

[19] Maurer C, Jesacher A, Bernet S, Ritsch-Marte M. What spatial light modulators can do for optical microscopy. Laser Photon Rev 2011;5(1):81–101.
[20] Jesacher A, Fürhapter S, Bernet S, Ritsch-Marte M. Spiral interferogram analysis. J Opt Soc Am A 2006;23:6.
[21] Aguilar A, Dávila A, García-Márquez J. Multi-step vortex filtering for phase extraction. Optics Expr 2014;22(7):8503–14.
[22] Du Y, Zhao H, Zhao Z. Sign-singularity solution in single-frame speckle interferometry with vortex-phase modulation. Optics Lett 2022;47:11.
[23] Goodman JW. Introduction to Fourier Optics. New York: McGraw-Hill; 1996.
[24] Coupland JM, Halliwell NA. A k-space analysis of holographic particle image velocimetry. Asian J Phy 2006;15(3):211–22.
[25] Coupland J M, Lobera J. Holography, tomography and 3D microscopy as linear filtering operations. Meas Sci Technol 2008;19:074012. https://doi.org/10.1088/0957-0233/19/7/074012.